UNTANGLING THE DYNAMICS OF SOIL-STRUCTURE INTERACTION USING NONLINEAR FINITE ELEMENT MODEL UPDATING

Hamed Ebrahimian[1], Domniki Asimaki[2], Danilo Kusanovic[3] and S. Farid Ghahari[4]

[1] Scientific Research Assistant, Department of Mechanical and Civil Engineering, Caltech
[2] Professor, Department of Mechanical and Civil Engineering, Caltech
[3] Ph.D. Candidate, Department of Mechanical and Civil Engineering, Caltech
[4] Postdoctoral Researcher, Department of Civil and Environmental Engineering, UCLA

Abstract

The dynamic response of a building structure to an earthquake excitation is the result of a complex interaction between the structural system and the underlying and surrounding geology. Since modeling the physics of the coupled soil-structure system is a complex undertaking, the state-of-practice has adopted simplified modeling procedures, such as the substructure method. Nevertheless, these procedures are often empirical and/or based on idealized assumptions, such as linear-elasticity. In this study, our objective is to develop a robust model inversion framework that can be utilized to extract information from the real-world building response measurements to back-calculate the model parameters that characterize the structural response and soil-structure interaction effects.

Introduction

The dynamic response of a building structures to an earthquake excitation is the result of a complex interaction between the structural system and the underlying and surrounding geology. The coupled soil-structure response is a function of seismic waves interacting with the building foundation, the nonlinear structural and geologic material response, and other energy dissipation mechanisms such as friction and viscous damping in the structure and soil. Therefore, the prediction accuracy of structural response quantities depends on the accuracy of the employed numerical model in characterizing these different sources of seismic energy dissipation and the dynamic soil-structure interaction.

Since modeling the physics of the coupled soil-structure system in detail is a complex undertaking, especially for practical design or assessment purposes, the state-of-practice has adopted simplified modeling procedures (e.g., [1], [2]). Soil-structure interaction effects are usually modeled using a substructure approach, where the soil flexibility and energy dissipation are modeled using distributed springs and dashpots [3]. Numerous simplified solutions exist to determine the stiffness and damping coefficients of these elements; solutions that are nonetheless based on idealized and restrictive assumptions. Examples of these assumptions include linear-elastic soil and structural behavior, uniform soil half space (or soil profiles with stiffness gradually varying with depth [4]), canonical foundation geometry, etc. These assumptions and the empirical nature of mechanical analogs such as soil springs and dashpots, could potentially lead to large error margins in predicting the seismic response of real-world building structures, even if the simplified models have demonstrated acceptable accuracy for ideal cases. The

applicability of these models becomes even more questionable for nonlinear response time history analyses. This is due to the fact that the concept of soil impedance functions and the resulting equivalent soil springs and dashpot is mainly based on the premise of linear-elastic response behavior. Nevertheless, the coupled soil-structure system is expected to experience nonlinearity during strong earthquakes – both material and geometrical (e.g., foundation-soil separation during rocking). Thus, the system may deviate substantially from the underlying assumptions that have led to substructure modeling techniques for soil-structure interaction analysis.

On the other hand, modern seismic design and assessment codes are progressively stirring toward nonlinear finite element (FE) modeling and response simulations for predictions of structural and nonstructural seismic demands. In a modern seismic analysis approach, a well-calibrated nonlinear model is required to precisely predict not only the peak values of response parameters, but also the time histories of structural responses. Despite all the advancements made in the field of mechanics-based nonlinear structural modeling, the state-of-practice for modeling structural damping and soil-structure interaction is still based on empirical assumptions. Clearly, there is an inconsistency between the mechanics-based modeling techniques available for structural systems and the underlying assumptions guiding the structural damping and soil-structure interaction modeling. This could result in an "inconsistent crudeness" in state-of-the-art seismic modeling of building structures that this proposal seeks to investigate.

In this study, we do not seek to develop new models of soil springs and dashpots or structural damping. Instead, we seek developing a model inversion framework that can be utilized to extract information from the real-world building response measurements to back-calculate the model parameters that characterize the structural response and soil-structure interaction effects. By repeating this effort for different building case studies and earthquake records in the long run, our objective is to compare the estimation results with the state-of-the-art recommendations, and to provide guidelines on how to improve the state-of-practice structural modeling capabilities.

Model Inversion through Nonlinear FE Model Updating

Suppose that the dynamic response of a building structure is recorded during an earthquake event. To simulate the dynamic response of this building structure, a mechanics-based (linear or nonlinear) FE model is developed. The FE model depends on a set of unknown parameters including inertia properties, damping parameters, soil spring and dashpot parameters, and parameters characterizing the nonlinear material constitutive laws used in the FE model. These parameters are referred to as the model parameters henceforth. Using the recorded input ground acceleration time history and the response of the building, the objective is to identify the best set of unknown model parameters that minimize the discrepancy between FE predicted and measured structural responses. Another objective of is to utilize the measured structural responses to jointly estimate the model parameters and input excitation (i.e., foundation input motion) time history.

In this study, the estimation problem is tackled by updating sequentially (i.e., for several batch of measurement data) the probability distribution function (PDF) of the unknown model parameters (and input excitation) using a Bayesian inference method (e.g., [5], [6]). FE model

updating using the measured input excitation and output response of the structure is referred to as the input-output model updating. Contrarily, in an output-only FE model updating, one or multiple time histories of the dynamic input excitation are also unknown. Therefore, the objective of the sequential Bayesian estimation is to estimate jointly the FE model parameters and the time unknown time history of the base excitation so that the discrepancies between the estimated and measured response quantities are minimized [7].

Background

The time-discretized equation of motion of a nonlinear FE model at time step i ($i = 1 \to k$, where *k* denotes the total number of time steps) is expressed as

$$\mathbf{M}(\boldsymbol{\theta})\,\ddot{\mathbf{q}}_i(\boldsymbol{\theta}) + \mathbf{C}(\boldsymbol{\theta})\,\dot{\mathbf{q}}_i(\boldsymbol{\theta}) + \mathbf{r}_i(\mathbf{q}_i(\boldsymbol{\theta}), \boldsymbol{\theta}) = \mathbf{f}_i(\boldsymbol{\theta}) \tag{1}$$

where $\mathbf{M}(\boldsymbol{\theta}) \in \mathrm{P}^{n_{DOF} \times n_{DOF}}$ = mass matrix, $\mathbf{C}(\boldsymbol{\theta}) \in \mathrm{P}^{n_{DOF} \times n_{DOF}}$ = damping matrix, $\mathbf{r}_i(\mathbf{q}_i(\boldsymbol{\theta}), \boldsymbol{\theta}) \in \mathrm{P}^{n_{DOF} \times 1}$ = history-dependent (or path-dependent) internal resisting force vector, $\mathbf{q}_i(\boldsymbol{\theta}), \dot{\mathbf{q}}_i(\boldsymbol{\theta}), \ddot{\mathbf{q}}_i(\boldsymbol{\theta}) \in \mathrm{P}^{n_{DOF} \times 1}$ = nodal displacement, velocity, and acceleration response vectors, respectively, $\boldsymbol{\theta} \in \mathrm{P}^{n_{\boldsymbol{\theta}} \times 1}$ = FE model parameter vector, $\mathbf{f}_i(\boldsymbol{\theta}) \in \mathrm{P}^{n_{DOF} \times 1}$ = dynamic load vector, and n_{DOF} = number of degrees-of-freedom. In the case of uniform (or rigid) seismic base excitation, $\mathbf{f}_i(\boldsymbol{\theta}) = -\mathbf{M}(\boldsymbol{\theta})\mathbf{L}\ddot{\mathbf{u}}_i^g$ where $\mathbf{L} \in \mathrm{P}^{n_{DOF} \times n_{\ddot{\mathbf{u}}^g}}$ = base acceleration influence matrix, and $\ddot{\mathbf{u}}_i^g \in \mathrm{P}^{n_{\ddot{\mathbf{u}}^g} \times 1}$ denotes the seismic input ground acceleration vector. Using a recursive numerical integration rule, such as the Newmark-beta method [8], Eq. (1) is reduced to a nonlinear vector-valued algebraic equation that can be solved recursively and iteratively in time to find the nodal response vector at each time step. In general, the response of a FE model at each time step is expressed as a function (linear or nonlinear) of the nodal displacement, velocity, and/or acceleration response vectors at that time step. Denoting the response quantity predicted by the FE model at time step *i* by $\hat{\mathbf{y}}_i \in \mathrm{P}^{n_{\mathbf{y}} \times 1}$, it follows that

$$\hat{\mathbf{y}}_i = \mathbf{h}_i\left(\boldsymbol{\theta}, \ddot{\mathbf{u}}_{1:i}^g, \mathbf{q}_0, \dot{\mathbf{q}}_0\right) \tag{2}$$

where $\mathbf{h}_i(...)$ is the nonlinear response function of the FE model at time step *i*. The measured response vector of the structure, $\mathbf{y}_i$, is related to the FE predicted response, $\hat{\mathbf{y}}_i$, as

$$\mathbf{v}_i\left(\boldsymbol{\theta}, \ddot{\mathbf{u}}_{1:i}^g\right) = \mathbf{y}_i - \hat{\mathbf{y}}_i\left(\boldsymbol{\theta}, \ddot{\mathbf{u}}_{1:i}^g\right) \tag{3}$$

in which $\mathbf{v}_i \in \mathrm{P}^{n_{\mathbf{y}} \times 1}$ is the simulation error vector and accounts for the misfit between the measured and FE predicted response of the structure. This misfit stems from the output measurement noise, parameter uncertainty, and model uncertainties. The latter stands for the mathematical idealizations and imperfections underlying the FE model, which result in an inherent misfit between the FE model prediction and the measured structural response [9]. In the absence of model uncertainties, it is assumed here that the measurement noises are stationary, zero-mean, independent Gaussian white noise processes (i.e., statistically independent across

time and measurement channels) [10]. Therefore, the probability distribution function (PDF) of the simulation error in Eq. (3) is expressed as

$$p(\mathbf{v}_i) = \frac{1}{(2\pi)^{n_y/2} |\mathbf{R}|^{1/2}} e^{-\frac{1}{2}\mathbf{v}_i^T \mathbf{R}^{-1} \mathbf{v}_i} \tag{4}$$

in which $|\mathbf{R}|$ denotes the determinant of the diagonal matrix $\mathbf{R} \in \mathrm{P}^{n_y \times n_y}$, which is the (time-invariant) covariance matrix of the simulation error vector (i.e., $\mathbf{R} = E(\mathbf{v}_i \mathbf{v}_i^T)$, $\forall i$).

In an output-only FE model updating problem, the FE model parameter vector ($\boldsymbol{\theta}$) and the time history of the seismic input ground acceleration at each time step ($\ddot{\mathbf{u}}_{1:k}^g$) are unknown and modeled as random variables (the corresponding random variables are denoted by $\boldsymbol{\Theta}$ and $\ddot{\mathbf{U}}_{1:k}^g$, respectively). Using Bayes' rule, the posterior probability distribution of the unknowns can be expressed as

$$p\left(\boldsymbol{\theta}, \ddot{\mathbf{u}}_{1:k}^g \mid \mathbf{y}_{1:k}\right) = \frac{p\left(\mathbf{y}_{1:k} \mid \boldsymbol{\theta}, \ddot{\mathbf{u}}_{1:k}^g\right) p\left(\boldsymbol{\theta}, \ddot{\mathbf{u}}_{1:k}^g\right)}{p\left(\mathbf{y}_{1:k}\right)} \tag{5}$$

where $p\left(\mathbf{y}_{1:k} \mid \boldsymbol{\theta}, \ddot{\mathbf{u}}_{1:k}^g\right) = p(\mathbf{v}_{1:k})$ = likelihood function, $p\left(\boldsymbol{\theta}, \ddot{\mathbf{u}}_{1:k}^g\right)$ = joint prior distribution of the random variables $\boldsymbol{\Theta}$ and $\ddot{\mathbf{U}}_{1:k}^g$, and $p(\mathbf{y}_{1:k})$ = normalizing constant independent of $\boldsymbol{\Theta}$ and $\ddot{\mathbf{U}}_{1:k}^g$. The objective of the output-only FE model updating problem is to estimate jointly the unknown model parameters and the ground acceleration time history such that their joint posterior PDF given the measured response of the structure is maximized, i.e.,

$$\left(\hat{\boldsymbol{\theta}}, \hat{\ddot{\mathbf{u}}}_{1:k}^g\right)_{\mathrm{MAP}} = \underset{\left(\boldsymbol{\theta}, \ddot{\mathbf{u}}_{1:k}^g\right)}{\arg\max}\ p\left(\boldsymbol{\theta}, \ddot{\mathbf{u}}_{1:k}^g \mid \mathbf{y}_{1:k}\right) \tag{6}$$

in which $\mathbf{y}_{1:k} = \left[\mathbf{y}_1^T, \mathbf{y}_2^T, ..., \mathbf{y}_k^T\right]^T$ = time history of the measured response of the structure, and MAP stands for the maximum posterior estimate. The estimation uncertainty is quantified by evaluating the parameter estimation covariance matrix at the MAP estimate.

Since the model inversion problem is highly nonlinear, a sequential estimation approach, referred to as the sequential Bayesian estimation method, is used in this study to improve the computational efficiency and convergence rate. In this approach, the estimation time interval is divided into successive overlapping time windows, referred to as the estimation windows. The estimation problem is solved at each estimation window to estimate the posterior PDF of unknown parameters. The first two moment of distribution (i.e., mean vector and covariance matrix) of the parameters are then transferred to the next estimation window and used as prior information. The sequential Bayesian estimation method approach is schematically shown in Figure 1. Two approaches are developed to find the posterior mean vector and covariance matrix of the unknown parameters and from the prior estimates: (i) a FE model linearization approach,

and (ii) an unscented transformation approach. These two methods are described in the next two sections, respectively.

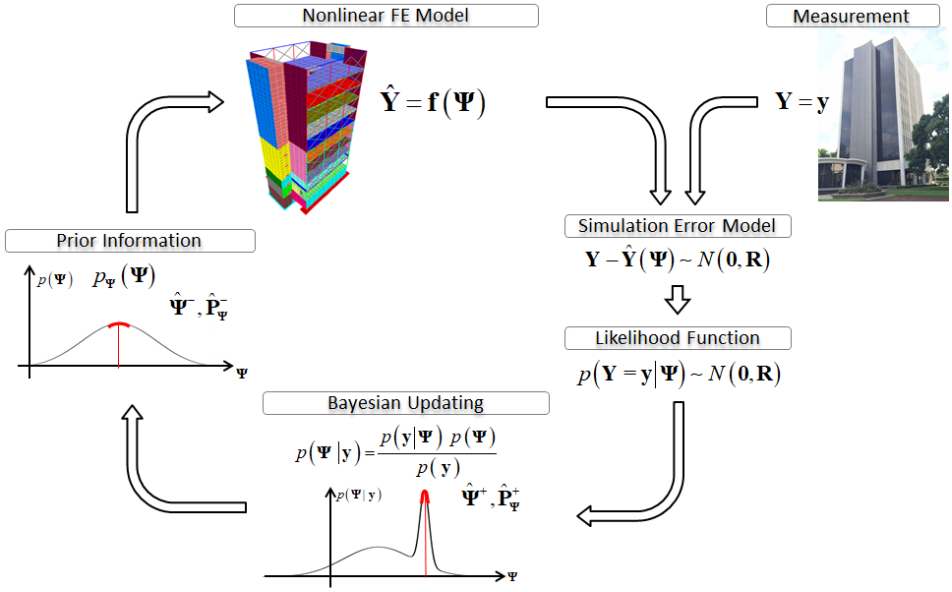

Figure 1: Schematic presentation of the sequential Bayesian FE model updating method.

Sequential Bayesian Estimation using FE Model Linearization

Following Eq. (5) and the sequential estimation logic described above, the natural logarithm of the posterior joint PDF of the FE model parameters and base acceleration time history at the m^{th} estimation window, spanning from time step t_1^m to time step t_2^m, can be derived as

$$\log\left(p\left(\boldsymbol{\theta}, \ddot{\mathbf{u}}^{g,m}_{t_1^m:t_2^m} \middle| \mathbf{y}_{t_1^m:t_2^m}\right)\right) = c + \log\left(p\left(\mathbf{y}_{t_1^m:t_2^m} \middle| \boldsymbol{\theta}, \ddot{\mathbf{u}}^{g,m}_{t_1^m:t_2^m}\right)\right) + \log\left(p\left(\boldsymbol{\theta}, \ddot{\mathbf{u}}^{g,m}_{t_1^m:t_2^m}\right)\right) \tag{7}$$

in which $c = -\log\left(p\left(\mathbf{y}_{t_1^m:t_2^m}\right)\right)$ is a constant. In this equation, the time history of the base acceleration from time step 1 to $t_1^m - 1$, (i.e., $\ddot{\mathbf{u}}^g_{1:t_1^m-1}$), is assumed to be deterministic and equal to the mean estimates obtained from previous estimation sequences. For notational convenience, an extended parameter vector at the m^{th} estimation window is defined as $\boldsymbol{\psi}_m = \left[\boldsymbol{\theta}^T, \ddot{\mathbf{u}}^{g,m\ T}_{t_1^m:t_2^m}\right]^T$, where $\boldsymbol{\psi}_m \in \mathrm{P}^{\left(n_{\boldsymbol{\theta}} + t_l \times n_{\ddot{\mathbf{u}}^g}\right)\times 1}$. Since the simulation error is modeled as an independent Gaussian white noise process, the likelihood function is given by

$$p\left(\mathbf{y}_{1:k} \middle| \boldsymbol{\theta}, \ddot{\mathbf{u}}^g_{1:k}\right) = \prod_{i=1}^{k} p(\mathbf{v}_i) \tag{8}$$

$$\Rightarrow \boldsymbol{p}\left(\mathbf{y}_{1:k} \,\middle|\, \boldsymbol{\theta}, \ddot{\mathbf{u}}^{g}_{1:k}\right) = \prod_{i=1}^{k} \frac{1}{(2\pi)^{n_y/2} \left|\mathbf{R}\right|^{1/2}} \boldsymbol{e}^{-\frac{1}{2}\left(\mathbf{y}_i - \mathbf{h}_i\left(\boldsymbol{\theta}, \ddot{\mathbf{u}}^{g}_{1:i}, \mathbf{q}_0, \dot{\mathbf{q}}_0\right)\right)^T \mathbf{R}^{-1} \left(\mathbf{y}_i - \mathbf{h}_i\left(\boldsymbol{\theta}, \ddot{\mathbf{u}}^{g}_{1:i}, \mathbf{q}_0, \dot{\mathbf{q}}_0\right)\right)}$$

By substitution of Eq. (8) into Eq. (7) and assuming a Gaussian distribution for the prior joint PDF, it follows that

$$\log\left(\boldsymbol{p}\left(\boldsymbol{\psi}_m \middle| \mathbf{y}_{t_1^m:t_2^m}\right)\right) = \boldsymbol{k}_0 - \frac{1}{2}\left(\mathbf{y}_{t_1^m:t_2^m} - \mathbf{h}_{t_1^m:t_2^m}\left(\boldsymbol{\psi}_m, \hat{\ddot{\mathbf{u}}}^{g}_{1:t_1^m-1}\right)\right)^T \tilde{\mathbf{R}}^{-1}\left(\mathbf{y}_{t_1^m:t_2^m} - \mathbf{h}_{t_1^m:t_2^m}\left(\boldsymbol{\psi}_m, \hat{\ddot{\mathbf{u}}}^{g}_{1:t_1^m-1}\right)\right) - \cdots$$
$$\frac{1}{2}\left(\boldsymbol{\psi}_m - \hat{\boldsymbol{\psi}}_m^{-}\right)^T \left(\hat{\mathbf{P}}_{\psi}^{-}\right)^{-1}\left(\boldsymbol{\psi}_m - \hat{\boldsymbol{\psi}}_m^{-}\right) \tag{9}$$

where $\boldsymbol{k}_0$ is a constant, and $\hat{\boldsymbol{\psi}}_{\boldsymbol{m}}^{-}$ and $\hat{\mathbf{P}}_{\boldsymbol{\psi}}^{-}$ are the prior mean vector and covariance matrix of the extended parameter vector at the m^{th} estimation window. $\tilde{\mathbf{R}} \in \mathrm{P}^{(t_l \times n_y)\times(t_l \times n_y)}$ is a block diagonal matrix, in which the diagonals are the simulation error covariance matrix $\mathbf{R}$. To find the MAP estimate of $\boldsymbol{\psi}_{\boldsymbol{m}}$, the posterior PDF in Eq. (9) is maximized, i.e.,

$$\frac{\partial \log\left(\boldsymbol{p}\left(\boldsymbol{\psi}_m \middle| \mathbf{y}_{t_1^m:t_2^m}\right)\right)}{\partial \boldsymbol{\psi}_m} = \mathbf{0} \Rightarrow$$

$$\left(\frac{\partial \mathbf{h}_{t_1^m:t_2^m}\left(\boldsymbol{\psi}_m, \hat{\ddot{\mathbf{u}}}^{g}_{1:t_1^m-1}\right)}{\partial \boldsymbol{\psi}_m}\right)^T \tilde{\mathbf{R}}^{-1}\left(\mathbf{y}_{t_1^m:t_2^m} - \mathbf{h}_{t_1^m:t_2^m}\left(\boldsymbol{\psi}_m, \hat{\ddot{\mathbf{u}}}^{g}_{1:t_1^m-1}\right)\right) - \left(\hat{\mathbf{P}}_{\psi}^{-}\right)^{-1}\left(\boldsymbol{\psi}_m - \hat{\boldsymbol{\psi}}_m^{-}\right) = 0 \tag{10}$$

Eq. (10), which is a nonlinear algebraic equation in $\boldsymbol{\psi}_m$ can be solved using an iterative first order approximation of the FE response function $\mathbf{h}_{t_1^m:t_2^m}\left(\boldsymbol{\psi}_m, \ddot{\mathbf{u}}^{g}_{1:t_1^m-1}\right)$ at $\hat{\boldsymbol{\psi}}_m^{-}$ as

$$\mathbf{h}_{t_1^m:t_2^m}\left(\boldsymbol{\psi}_m, \hat{\ddot{\mathbf{u}}}^{g}_{1:t_1^m-1}\right) = \mathbf{h}_{t_1^m:t_2^m}\left(\hat{\boldsymbol{\psi}}_m^{-}, \hat{\ddot{\mathbf{u}}}^{g}_{1:t_1^m-1}\right) + \left.\frac{\partial \mathbf{h}_{t_1^m:t_2^m}\left(\boldsymbol{\psi}_m, \hat{\ddot{\mathbf{u}}}^{g}_{1:t_1^m-1}\right)}{\partial \boldsymbol{\psi}_m}\right|_{\boldsymbol{\psi}_m = \hat{\boldsymbol{\psi}}_m^{-}} \left(\boldsymbol{\psi}_m - \hat{\boldsymbol{\psi}}_m^{-}\right) + \boldsymbol{H.O.T.} \tag{11}$$

The matrix $\left.\frac{\partial \mathbf{h}_{t_1^m:t_2^m}\left(\boldsymbol{\psi}_m, \ddot{\mathbf{u}}_{g\,1:t_1^m-1}\right)}{\partial \boldsymbol{\psi}_m}\right|_{\boldsymbol{\psi}_m = \hat{\boldsymbol{\psi}}_m^{-}}$ represents the FE response sensitivities with respect to the extended parameter vector, evaluated at the prior mean values of the extended parameter vector, $\hat{\boldsymbol{\psi}}_{\boldsymbol{m}}^{-}$. This matrix is denoted by $\mathbf{C}$ hereafter for notational convenience. Substituting Eq. (11) into Eq. (10) and neglecting the higher order terms results in the following (first order approximate) equation for the MAP estimate of $\boldsymbol{\psi}_m$:

$$\hat{\boldsymbol{\psi}}_{\boldsymbol{m}}^{+} = \hat{\boldsymbol{\psi}}_{\boldsymbol{m}}^{-} + \left(\mathbf{C}^{\boldsymbol{T}} \tilde{\mathbf{R}}^{-1} \mathbf{C} + \left(\hat{\mathbf{P}}_{\boldsymbol{\psi}}^{-}\right)^{-1}\right)^{-1} \mathbf{C}^{\boldsymbol{T}} \tilde{\mathbf{R}}^{-1}\left(\mathbf{y}_{t_1^m:t_2^m} - \mathbf{h}_{t_1^m:t_2^m}\left(\hat{\boldsymbol{\psi}}_{\boldsymbol{m}}^{-}, \hat{\ddot{\mathbf{u}}}^{g}_{1:t_1^m-1}\right)\right) \tag{12}$$

in which $\hat{\psi}_m^+$ is the updated (or the posterior) mean estimate of ψ_m. It can be shown that the term $\tilde{\mathbf{K}} = \left(\mathbf{C}^T \tilde{\mathbf{R}}^{-1} \mathbf{C} + \left(\hat{\mathbf{P}}_{\Psi}^- \right)^{-1} \right)^{-1} \mathbf{C}^T \tilde{\mathbf{R}}^{-1}$ is similar to the Kalman gain matrix, as used for Kalman filtering [11].

The updated $\hat{\psi}_m^+$ from Eq. (12) is iteratively used as the new point for the linearization of the nonlinear FE model in Eq. (11) to find an improved estimation. This iterative prediction-correction procedure at each estimation window is equivalent to an iterative EKF method for parameter-only estimation [11]. Following the EKF procedure, the prior covariance matrix of the extended parameter vector $\hat{\mathbf{P}}_{\Psi,m}^-$ is updated to the posterior covariance matrix $\hat{\mathbf{P}}_{\Psi,m}^+$ after each prediction-correction iteration. Moreover, it is assumed that both the prior and posterior joint PDF of the extended parameter vector are Gaussian. The updated estimation covariance matrix, can be derived as

$$\hat{\mathbf{P}}_{\psi,m}^+ = \boldsymbol{E}\left[\left(\boldsymbol{\Psi}_m - \hat{\boldsymbol{\psi}}_m^+ \right) \left(\boldsymbol{\Psi}_m - \hat{\boldsymbol{\psi}}_m^+ \right)^T \right] = \left(\mathbf{I} - \mathbf{KC} \right) \hat{\mathbf{P}}_{\psi,m}^- \left(\mathbf{I} - \mathbf{KC} \right)^T + \mathbf{K} \tilde{\mathbf{R}} \mathbf{K}^T \tag{13}$$

Furthermore, to improve the convergence of the iterative prediction-correction procedure, a constant disturbance matrix is added to the posterior covariance matrix at each iteration to provide the prior covariance matrix for the next iteration, i.e.,

$$\hat{\mathbf{P}}_{\Psi,i+1}^- = \hat{\mathbf{P}}_{\Psi,i}^+ + \mathbf{Q} \tag{14}$$

where $\mathbf{Q}$ is a constant diagonal matrix with small positive diagonal entries (relative to the diagonal entries of matrix $\hat{\mathbf{P}}_{\Psi,i}^+$). The matrix $\mathbf{Q}$ is referred to as process noise covariance matrix in the Kalman filtering world. The subscript *i* in Eq. (14) denotes the iteration number.

Sequential Bayesian Estimation using the Unscented Transformation

While the terms $\hat{\mathbf{P}}_{\psi\mathbf{y}}$ = cross-covariance matrix of $\boldsymbol{\Psi}$ and $\mathbf{Y}$, and $\hat{\mathbf{P}}_{\mathbf{yy}}$ = covariance matrix of $\mathbf{Y}$ in are derived by linearizing the nonlinear FE model in the previous section, an unscented transformation (UT) method (e.g., [12], [13]) can also be used to derive the $\hat{\mathbf{P}}_{\psi\mathbf{y}}$ and $\hat{\mathbf{P}}_{\mathbf{yy}}$. UT is a deterministic sampling approach to propagate the uncertainty in $\boldsymbol{\Psi}$ through the nonlinear FE model; thus, circumventing the linearization of the FE model. Therefore, it results in a more accurate estimation of the $\hat{\mathbf{P}}_{\psi\mathbf{y}}$ and $\hat{\mathbf{P}}_{\mathbf{yy}}$, especially for highly nonlinear models. Indeed, using the UT method is at the cost of evaluating the FE model at multiple samples of the vector $\boldsymbol{\Psi}$; nevertheless, the additional FE computations can be performed in parallel ([14], [15]).

In this approach, the nonlinear FE model is evaluated separately at a set of deterministically selected realizations of the extended parameter vector $\boldsymbol{\Psi}$, referred to as the sigma points (SPs) denoted by ϑ^j, which are selected around the prior mean estimate $\hat{\boldsymbol{\Psi}}^-$. In this study, a scaled UT based on $(2 \times \boldsymbol{n}_{\boldsymbol{\Psi}} + 1)$ sigma points (i.e., $\boldsymbol{j} = 1, 2, \ldots, (2 \times \boldsymbol{n}_{\boldsymbol{\Psi}} + 1)$) is used, where $\boldsymbol{n}_{\boldsymbol{\Psi}}$ denotes the size of the extended parameter vector. The mean and covariance matrix of

the FE predicted structural response $\mathbf{Y}$, and the cross-covariance matrix of $\mathbf{\Psi}$ and $\mathbf{Y}$ are respectively computed using a weighted sampling method as

$$\bar{\mathbf{y}} = \sum_{j=1}^{2\times n\Psi+1} W_m^j \, \hat{\mathbf{y}}\left(\vartheta^j\right) \tag{15}$$

$$\hat{\mathbf{P}}_{yy} = \sum_{j=1}^{2\times n\Psi+1} W_e^j \left[\hat{\mathbf{y}}\left(\vartheta^j\right) - \bar{\mathbf{y}}\right]\left[\hat{\mathbf{y}}\left(\vartheta^j\right) - \bar{\mathbf{y}}\right]^T + \mathbf{R} \tag{16}$$

$$\hat{\mathbf{P}}_{\Psi y} = \sum_{j=1}^{2\times n\Psi+1} W_e^j \left[\vartheta^j - \hat{\mathbf{\Psi}}^-\right]\left[\hat{\mathbf{y}}\left(\vartheta^j\right) - \bar{\mathbf{y}}\right]^T \tag{17}$$

where W_m^j and W_e^j denote the mean and covariance weighting coefficients, respectively [13]. With this approach, the Kalman gain matrix can be computed and the sequential parameter estimation can be pursued following Eqs. (12) and (13).

FE Model Updating of the Millikan Library Building

The Millikan Library

The Millikan Library is a reinforced concrete shear wall building with a basement level and nine stories above the ground. It is located on the California Institute of Technology (Caltech) campus in Pasadena, and was constructed from 1966 to 1967. Millikan library has been the subject of several studies, especially in the fields of system identification and structural health monitoring. The building is a unique case for soil-structure interaction studies, due to its unique structural and soil properties (Figure 2).

The Millikan Library structure is 43.9 m tall above ground including the roof level. It has a 4.3 m deep basement below the ground level. Except for the first and the roof levels, which are 4.9 m high, all floors are 4.3 m high. The basement is encased by surrounding retaining shear walls. A surrounding precast concrete wall enlaces the roof story to protect the installed mechanical equipment. The lateral force resisting system comprises of shear walls in the NS direction on the east and west sides of the building, and shear walls around the elevator shaft in the north-south and east-west directions. The floor system consist of lightweight reinforced concrete slabs supported by reinforced concrete beams. The foundation system consist of a 1.2 m deep central pad 6 meters below the ground level, and two foundation beams in the north and south sides of the building 5 meters below the ground level. Four stepped beams connect the foundation pad to the north and south foundation beams. This special foundation system acts somehow similar to a rocking chair [16].

FE Model Development

Using the available structural drawings, a detailed FE model of the structural system is developed. We used the graphic-user-interface of SAP2000 software [17] to develop the initial geometry of the model. The SAP2000 model was then transformed to OpenSees [18] using a series of custom-developed Matlab interfaces based on the SAP2000 Application Programming

Interface (API). The developed FE model in OpenSees is nonlinear, with an option to switch to a linear model. The model is based on fiber-section force-based beam-column elements to model beams and columns. Kent-Scott-Park uniaxial material model with linear tension softening is used to model concrete and Giuffré-Menegotto-Pinto material is utilized to model reinforcing steel. A multi-layered nonlinear shell element with damage-plasticity concrete material model [19] is used to model shear walls and slabs. The kinematic interaction of precast claddings on the north and south faces of the building with the structural system are modeled using diagonal brace elements, with an elastic-perfectly plastic material model. The brace elements are assumed to have a rectangular cross section of 0.1 x 0.1 m. By adjusting the elastic modulus and yield strength of their material model, the stiffness and force contribution of the precast panels to the dynamic response of the structure are modeled.

Figure 3 shows the geometry of the model. Different colors in this figure present different section properties used to define the shell (shear wall and slab) and beam-column elements. The model is meshed manually to adjust the size and shape of elements. It consists of 1,885 frame elements, 4,043 shell elements, and 27,526 digress of freedom.

Figure 2: Millikan Library building.

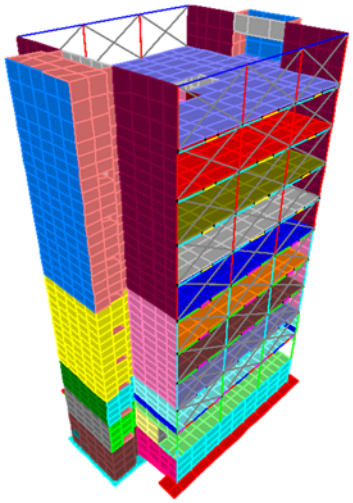

Figure 3: Developed FE model of the Millikan Library structure.

Several earthquake records are available for the Millikan Library. Details about sensor arrangements [20] and recorded earthquake data [16] are available in the literature and are not repeated here for brevity. For the purpose of this study, we used only the 2002 Yorba Linda earthquake record, which is a low-amplitude earthquake (PGA ~ 0.8% g). Although the level of considered earthquake in this study is low and therefore, may not activate the material nonlinearity, the developed model updating process is general and can be used with linear and or nonlinear models regardless of the earthquake intensity.

FE Model Updating using Foundation-Level Input Motions

At this stage, we use the measured acceleration response at the foundation level (i.e., foundation-level input motion) and the measured output response of the structure for the FE model updating. The objective of this input-output model updating is to estimate the unknown

model parameters of the superstructure, regardless of the soil subsystem. For this purpose, we start with an identifiability analysis to determine the most identifiable parameter sets. After selecting the parameter sets, we verify the estimation algorithms using simulated data. Finally, we use the real measurement data to estimate the model parameters.

Model Identifiability and Parameter Selection

Identifiability analysis is an approach to investigate if the unknown parameters can be uniquely estimated from data. To assess the parameter identifiability we used an information-theoretic approach [21] to measure the amount of information contained in measurement data about an unknown model parameter. The entropy gain is used to quantify the amount of information each unknown parameter receives from the measurement data. Comparing the entropy gain between different parameters is used to assess the relative identifiability of parameters. Moreover, the mutual entropy gain between parameter pairs is used to investigate the relative correlation between the parameters. This entropy gain and mutual entropy gain are used to guide the selection of the estimation parameters.

To assess the identifiability of model parameters, first we start with a nonlinear FE model. Twenty different parameters that characterize the material and inertia properties of model are selected, as shown in Table 1. Since the amplitude of the 2002 Yorba Linda earthquake is low, material yielding is not expected and therefore, only the elastic-related material parameters for reinforcing steel are included in the identifiability analysis. On the contrary, since the precast cladding are expected to yield under small inter-story drift ratios, the yield strength of brace elements is included in the analysis.

For a given input motion, the entropy gain for each parameter is a function of the initial (prior) value of the parameter, which is unknown in advance. The incorrect selection of the prior model parameter values can result in an incorrect identifiability assessment. Therefore, without the knowledge of correct parameter values, the identifiability assessment results would not be accurate anyways; but we still expect to have an approximate assessment of the identifiability. Initial material parameter values for steel and concrete are selected based on the material properties reported in the as-built drawings. The distributed floor mass (aside from self-mass of the structural materials) are estimated based on the approximate mass contribution of nonstructural components and live loads, and are in agreement with the building mass reported in [22]. The mass of each precast cladding panel is approximated as 5,000 kg based on Kuroiwa [22]. The stiffness, of the brace elements (used to model the kinematic interaction effects of the claddings) are approximated based on the modal analysis results before and after their installation ([23], [24]). The yield strength of the brace elements is approximated based on the experimental literature on the precast cladding panels (e.g., [25]). It should be noted that the stiffness and strength contribution of precast panels depends highly on the connection and construction details. In the absence of any detailed information about the precast panels in the Millikan Library, we postulated its properties based on engineering judgement. The model parameter values used for identifiability assessment are listed in Table 1.

Table 1: Twenty model parameters used for the first-step identifiability assessment.

Parameter ID	Description	Value
1	Elastic modulus (*Es*) of steel rebar in beams	180 GPa
2	Compressive strength (f'_c) of concrete in beams	27.6 MPa
3	Tensile strength (f'_t) of concrete in beams	1.73 MPa
4	Elastic modulus (*Ec*) of slab concrete in 1st floor	21 GPa
5	Elastic modulus (*Ec*) of slab concrete in 2nd floor	21 GPa
6	Elastic modulus (*Ec*) of slab concrete in 3rd to 5th floors	21 GPa
7	Elastic modulus (*Ec*) of slab concrete in 6th to roof floors	21 GPa
8	Compressive strength (f'_c) of concrete in columns	34.5 MPa
9	Tensile strength (f'_t) of concrete in columns	1.94 MPa
10	Elastic modulus (*Ec*) of shear wall concrete in basement	21 GPa
11	Elastic modulus (*Ec*) of shear wall concrete in 1st story	21 GPa
12	Elastic modulus (*Ec*) of shear wall concrete in 3rd to 5th stories	21 GPa
13	Elastic modulus (*Ec*) of shear wall concrete in 6th to roof stories	21 GPa
14	Elastic modulus (*E*) of brace elements representing the precast claddings	25 GPa
15	Distributed floor mass (*m*) on 1st to 9th floors	400 kg/m^2
16	Distributed floor mass (*m*) on basement floor	200 kg/m^2
17	Distributed floor mass (*m*) on roof	300 kg/m^2
18	Yield strength (f_y) of brace elements representing the precast claddings	140 MPa
19	Mass-proportional Rayleigh damping coefficient	0.1508
20	Stiffness-proportional Rayleigh damping coefficient	0.0038

Figure 4 shows the entropy gain of these twenty parameters. The entropy gain (measured in Nats) is the amount of information that the measurement data (i.e., the model responses herein) carries about each model parameters. It can be seen that the entropy gain of parameters #16 (distributed floor mass on basement floor), and #18 (yield strength of brace elements) is zero, which means that the structural response (for this specific base excitation) is not sensitive to these parameters. Those parameters that have the higher entropy gain are more likely to be identifiable.

Figure 5 shows the mutual entropy gain between the parameter pairs. This figure is used to investigate the dependence between parameters, which is presented with dark colors: darker colors means stronger relative dependence. For example, Figure 5 that there are strong mutual dependence between parameters #9 (Tensile strength of concrete in columns), #10 (Elastic modulus of shear wall concrete in basement), #11 (Elastic modulus of shear wall concrete in 1st story), and #12 (Elastic modulus of shear wall concrete in 3rd to 5th stories). Moreover, there are some competing effects between these parameters and parameters #1 (elastic modulus of steel rebar in beams), #15 (distributed floor mass on 1st to 9th floors), and #17 (distributed floor mass on roof). This plot along with the plot presented in Figure 4 can be used to choose the estimation

parameters. The parameters that gain relatively small amount of information from the measurement dataset, or have strong dependencies on the other estimation parameters can be put aside (i.e., fixed) during the estimation process to enhance the estimation performance.

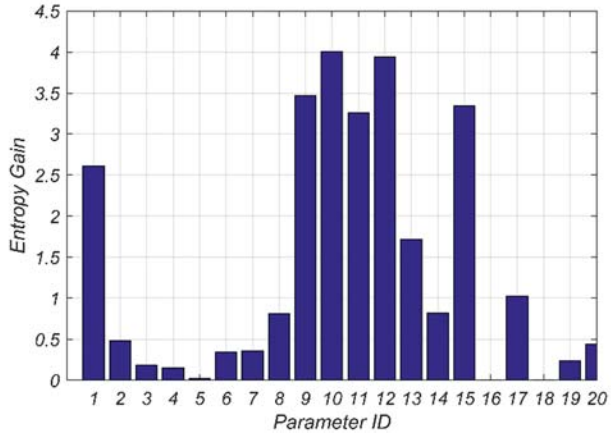

Figure 4: Entropy gain (in Nats) of the twenty model parameters.

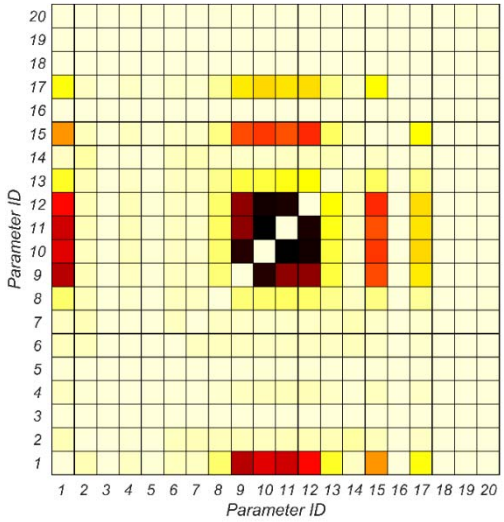

Figure 5: Relative mutual entropy gain between the parameter pairs.

Investigation of these two figures and the FE predicted response of the structure at the component-level reveals that the structure does not experience severe nonlinearity during this earthquake motion. Tensile cracking of concrete is expected in the columns (see parameter #9 in Figure 4), but no yielding is expected. Therefore, we decided to reduce the FE model to a linear elastic model for this earthquake excitation. Based on the presented results, we selected six final parameters to be estimated, as listed in Table 2. The initial (effective) elastic modulus values for concrete in this table are selected to account for tensile cracking under gravity loading.

Table 2: Final selected model parameters for linear-elastic model.

Parameter ID	Description	Value
1	Elastic modulus of brace elements representing the precast claddings (E_{Clad})	25 GPa
2	Elastic modulus of beams and slabs (all floors) (E_{floor})	15.8 GPa
3	Elastic modulus of shear wall and column concrete at 1st and 2nd stories ($E_{W\&C}1$)	22.1 GPa
4	Elastic modulus of shear wall and column concrete at 3rd to roof stories ($E_{W\&C}2$)	22.1 GPa
5	Stiffness-proportional Rayleigh damping coefficient (b)	0.0038
6	Distributed floor mass on 1st to 9th floors (m)	400 kg/m^2

Model Inversion using Recorded Yorba Linda Earthquake Data

After successful verification of the estimation algorithm, we utilize the real data recorded at the Millikan library building during the 2002 Yorba Linda earthquake for the model updating. The six unknown model parameters as introduced before are estimated. The initial and final estimate of parameters along with the final estimated coefficient of variation (COV) are listed in Table 3. Figure 6 shows the time history of the posterior mean and coefficient of variation (COV) of the model parameters, which presents the estimation uncertainties. To evaluate how well the updated model prediction matches the measurement records, Figure 7 compares the measured acceleration response time histories with those estimated using the initial and final estimates of the model parameters. Furthermore, Figure 8 compares the relative root mean square error (RRMSE) of the predicted FE model responses using the initial and final parameter estimates. This figure clearly shows that the model updating process has reduced the RRMSE substantially. Nevertheless, the time history plots in Figure 7 shows non-negligible differences between the estimated and measured response time histories, especially at the middle stories of the building and for the north-south acceleration responses. These differences are most likely due to the incorrect base rocking motions applied on the model. The rocking components of the base motion are calculated using the vertical accelerations recorded at different locations on the foundation level, and the (approximate) horizontal distance between the sensor locations. However, the vertical acceleration data are noisy and moreover, any approximation in determining the sensors' location may result in erroneous estimation of the rocking components of base acceleration. The effects of model uncertainty is another source of error that can contribute to the discrepancies between the estimated and measured structural responses in Figure 7.

Table 3: Initial and final estimate of model parameters using Yorba Linda earthquake data.

Parameter ID	Parameter	Initial Estimate	Final Estimate	Estimated COV (%)
1	E_{Clad}	20 GPa	7.81 GPa	1.60
2	E_{floor}	21 GPa	4.13 GPa	0.81
3	$E_{W\&C}1$	26.7 GPa	16.58 GPa	0.45
4	$E_{W\&C}2$	26.7 GPa	32.06 GPa	0.84
5	b	0.0038	0.0035	1.13
6	m	250 (kg/m^2)	153.84 (kg/m^2)	0.61

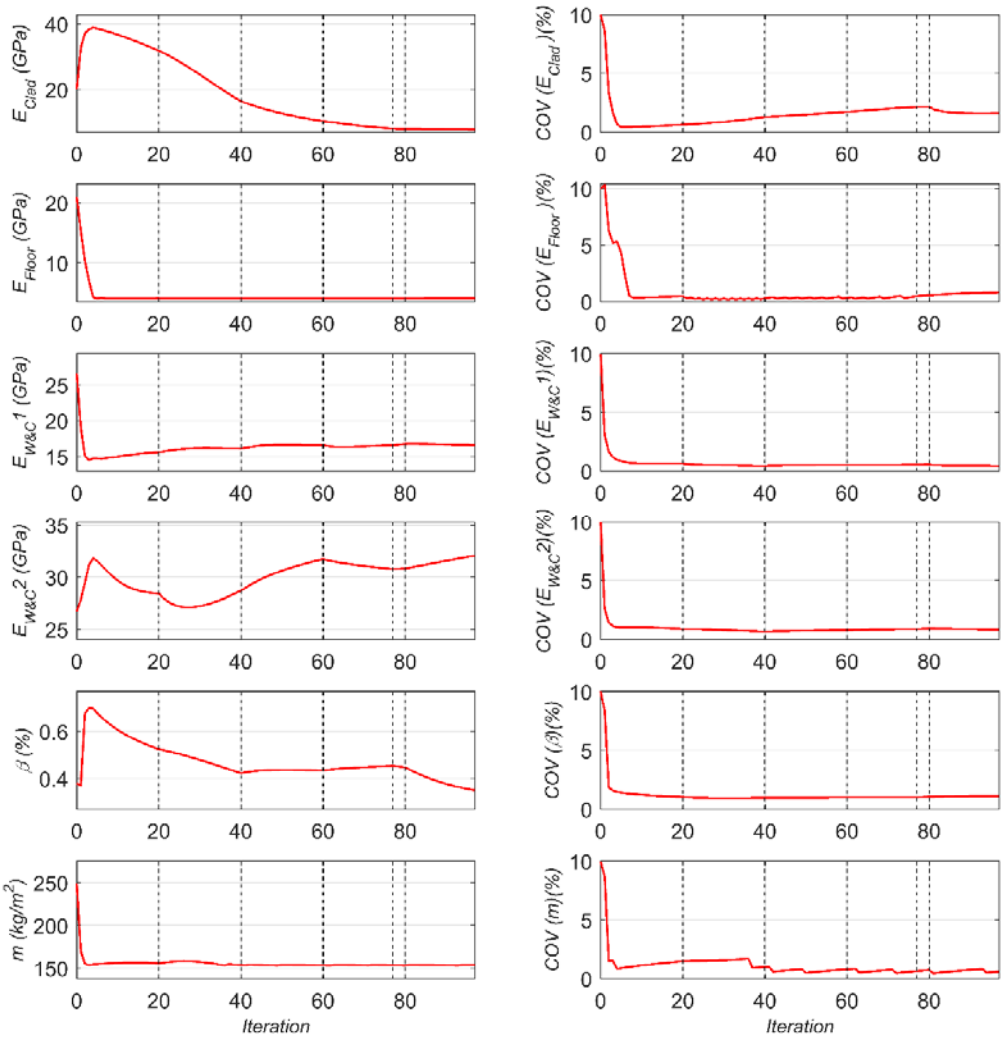

Figure 6: Time histories of the posterior mean (left) and coefficient of variation (COV) (right) of the model parameters estimated from the Yorba Linda earthquake records.

Output-Only Model Inversion

At this stage, we use the updated model of the superstructure, obtained from previous step, and the measured responses of the structure for an output-only FE model updating. The objective is to estimate the foundation input motions (FIMs) and the stiffness and viscosity of the soil springs and dashpots used to model the inertial soil-structure interaction effects. For this purpose, and similar to the previous step, we start with an identifiability analysis to evaluate the sensitivity of the structural response with respect to the soil stiffness and viscosity parameters. Then, we use the real measurement data to estimate the soil parameters.

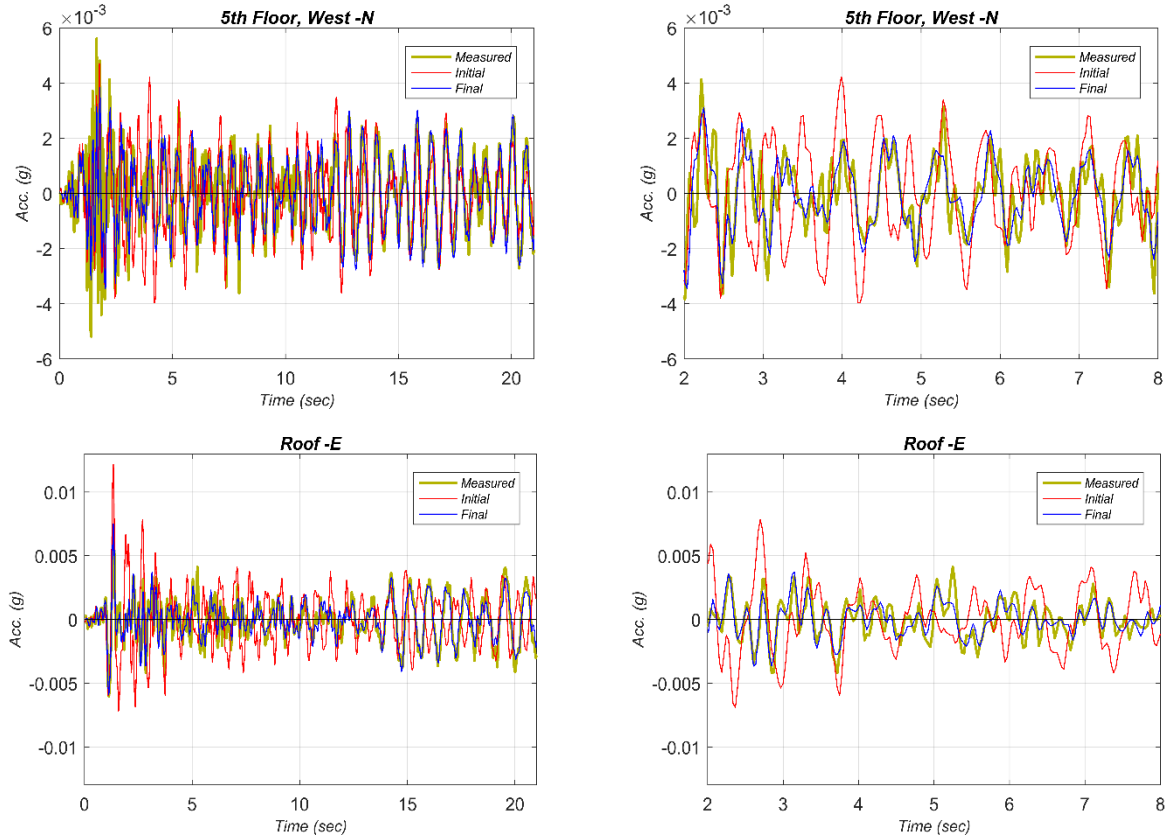

Figure 7: Comparison of the measured structural responses with the structural responses predicted using the initial and final estimate of model parameters.

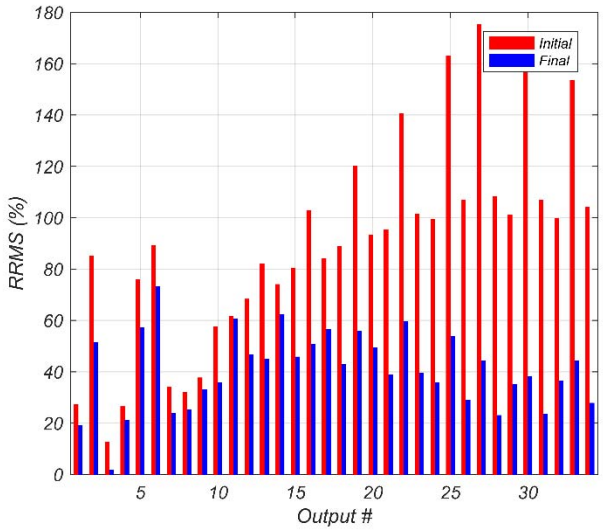

Figure 8: Relative root mean square error (RRMSE) of the FE predicted structural responses using the initial and final estimate of model parameters.

Model Identifiability and Parameter Selection

Distributed linear soil springs and dashpots are included underneath the foundation slab of the updated FE model, obtained from the previous step. Three linear springs and three linear viscous dashpots are modeled independently in x-, y-, and z-direction at each nodal point of the foundation slab. The stiffness of soil springs and viscosity of dashpots are computed using the subgrade modulus (i.e., soil stiffness per unit area), and viscosity modulus (i.e., viscosity of the soil per unit area), respectively, in x-, y-, and z-direction. The spring stiffness is calculated by multiplying the tributary area of the nodal point by the corresponding subgrade modulus. Similarly, the dashpot viscosity is calculated by multiplying the tributary area of the nodal point by the corresponding viscosity modulus.

Six different (unknown) subgrade modulus, namely k_x, k_y1, k_y2, k_z1, k_z2, k_z3, are defined for different foundation regions. These regions and the corresponding subgrade modules are shown Figure 9. Similarly, six (unknown) parameters are used to define the viscosity modulus of soil. The viscosity modulus parameters (c_x, c_y1, c_y2, c_z1, c_z2, c_z3) characterize the viscosity of the soil per unit area, and are specified in Figure 9.

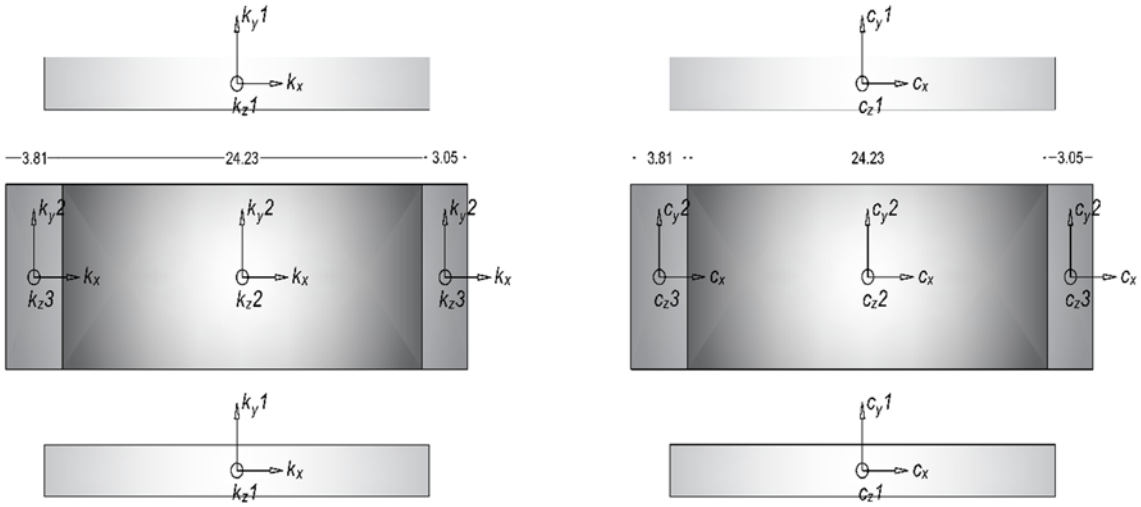

(a) (b)

Figure 9: (a) six unknown subgrade modulus parameters, and (b) six unknown viscosity modulus parameters defined for different foundation regions. The figure shows the foundation plan of the Millikan library including the central pad (at -6 m elevation), and the two foundation beams on the north and south sides (at -5 m elevation).

To assess the identifiability of these twelve soil parameters, we pursue the same identifiability analysis approach presented before. Initial estimate of soil model parameters are assigned following the results presented in [16], and the NIST standard recommendations [3], and are listed in Table 4.

Table 4: Twelve soil model parameters used for the first-step identifiability assessment.

Parameter ID	Description	Initial Estimate	Parameter ID	Description	Initial Estimate
1	k_x	65 MN/m^3	7	c_x	700 kN.s/m^3
2	k_y1	40 MN/m^3	8	c_y1	700 kN.s/m^3
3	k_y2	60 MN/m^3	9	c_y2	700 kN.s/m^3
4	k_z1	25 MN/m^3	10	c_z1	1000 kN.s/m^3
5	k_z2	22.5 MN/m^3	11	c_z2	1000 kN.s/m^3
6	k_z3	37.5 MN/m^3	12	c_z3	1000 kN.s/m^3

Figure 10 shows the entropy gain of the soil parameters. These plots presents the cumulative sensitivity of the FE model response (measured at 34 output channels) to the twelve soil parameters. The small entropy gain of some parameters such as k_y1, c_y1, c_z2, and c_z3 makes them weakly identifiable, and therefore these parameters are removed from the estimation process. Moreover, Figure 11, which shows the mutual entropy gain between the parameter pairs, indicates a strong dependence between k_z1, k_z2, and k_z3. This is not unexpected because the structural response does not include the vertical components of the acceleration (except on the foundation level). Therefore, although the rocking stiffness of the foundation system might be identifiable, its vertical stiffness remains weakly identifiable. By investigating these results, we decide to limit the number of estimation parameters to eight including: k_x, k_y, k_z1, k_z2, k_z3, c_x, c_y, and c_z. The three vertical stiffness are kept for the estimation despite their dependency.

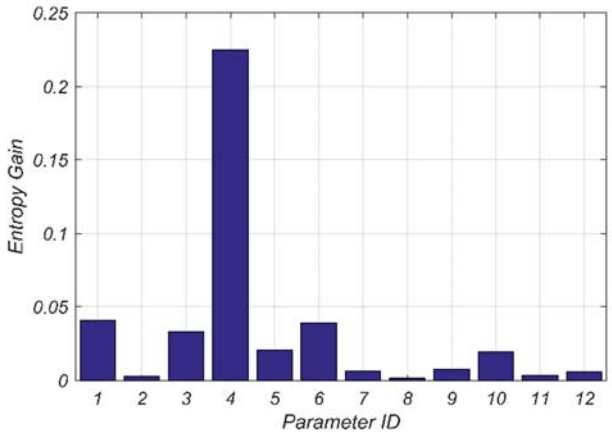

Figure 10: Entropy gain (in Nats) of the twelve soil parameters.

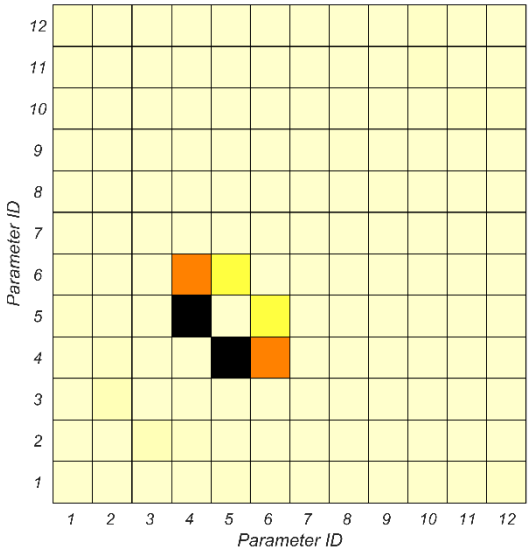

Figure 11: Relative mutual entropy gain between the soil parameter pairs.

Model Inversion using Recorded Yorba Linda Earthquake Data

The real data recorded at the Millikan library building during the 2002 Yorba Linda earthquake are now utilized for an output-only FE model updating to estimate the eight soil

parameters and the three components of the foundation input motion (FIM), namely in EW, NS, and Up directions. The initial and final estimate of parameters along with the estimated coefficient of variation (COV) are listed in Table 5. Figure 12 shows the time history of the three components of the estimated FIM. The estimation uncertainties are quantified through the standard deviation plots presented in this figure. Figure 13 shows the time history of the posterior mean and coefficient of variation (COV) of the soil parameters, which quantifies the estimation uncertainties. The large estimation uncertainties indicate the potential inaccuracy in the final parameter estimates. To evaluate how well the updated model prediction matches the measurement records, Figure 14 compares the measured acceleration response time histories with those estimated using the final estimates of the model parameters. This figure shows a remarkable match between the estimated and measured acceleration responses.

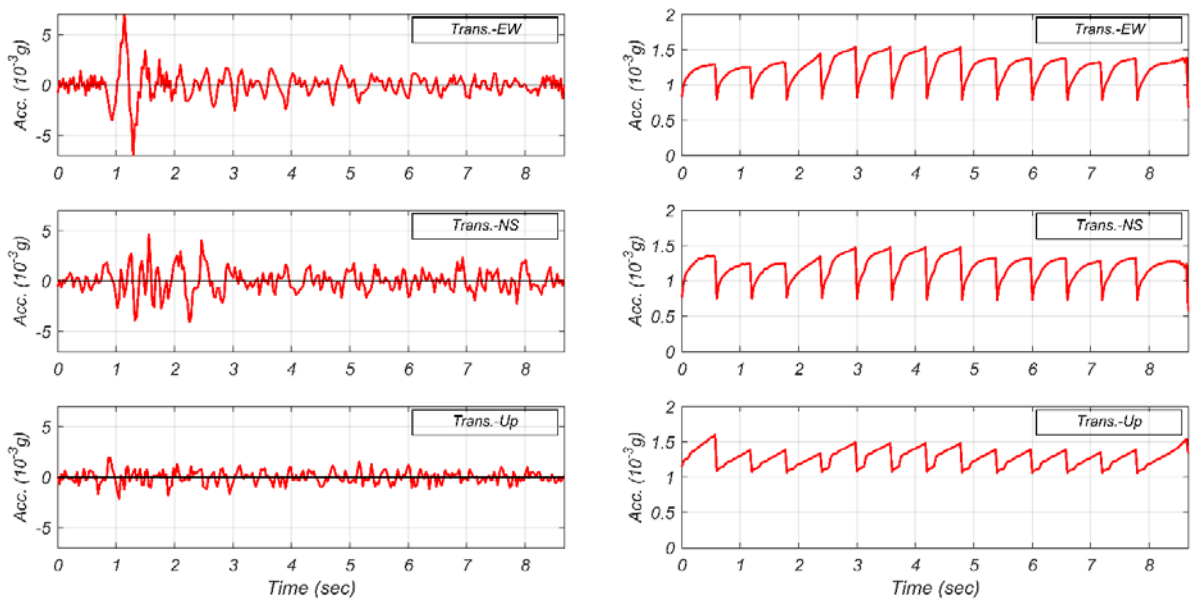

(a) (b)

Figure 12: Estimated foundation input motion (FIM) time history (left) and standard deviation (S.D.) of the estimated FIM time history (right).

Table 5: Initial and final estimates of soil parameters.

Parameter ID	Parameter	Initial Estimate	Final Estimate	Estimated COV (%)
1	k_x	65 MN/m^3	192.1 MN/m^3	19.4
2	k_y	50 MN/m^3	13.0 MN/m^3	40.3
3	k_z1	20 MN/m^3	106.6 MN/m^3	5.4
4	k_z2	22.5 MN/m^3	279.3 MN/m^3	14.4
5	k_z3	37.5 MN/m^3	408.8 MN/m^3	9.7
6	c_x	700 kN.s/m^3	2.4 MN.s/m^3	24.1
7	c_y	700 kN.s/m^3	1.8 MN.s/m^3	7.9
8	c_z	1000 kN.s/m^3	5.9 MN.s/m^3	4.9

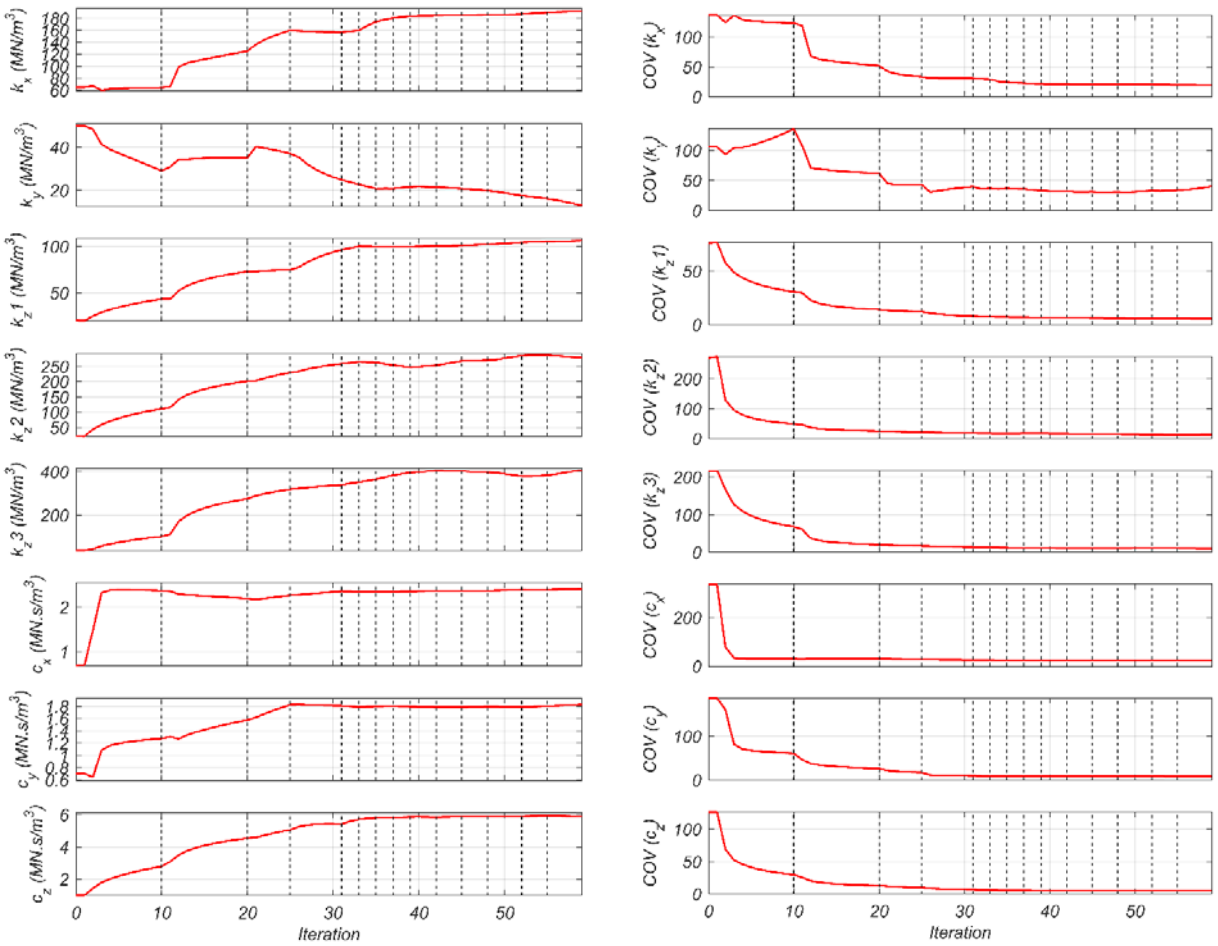

Figure 13: Time histories of the posterior mean (left) and coefficient of variation (COV) (right) of the model parameters estimated from the Yorba Linda earthquake records.

Summary and Conclusions

In this study, we developed a nonlinear FE model updating framework using a sequential Bayesian estimation approach based on the unscented transformation method. The FE model updating algorithm can estimate the unknown model parameters and/or the time history of dynamic input excitation using the measured structural responses. The algorithm can be used for input-output structural model updating (i.e., estimating the unknown model parameters using the foundation level input motion and the output response of the structure), and for output-only model updating (i.e., estimating jointly the unknown model parameters and the time history of input excitation). This capability has been used in this study to estimate the structural model parameters, the stiffness and viscosity of soil subsystem, and the foundation input motions (FIM) for the Millikan library.

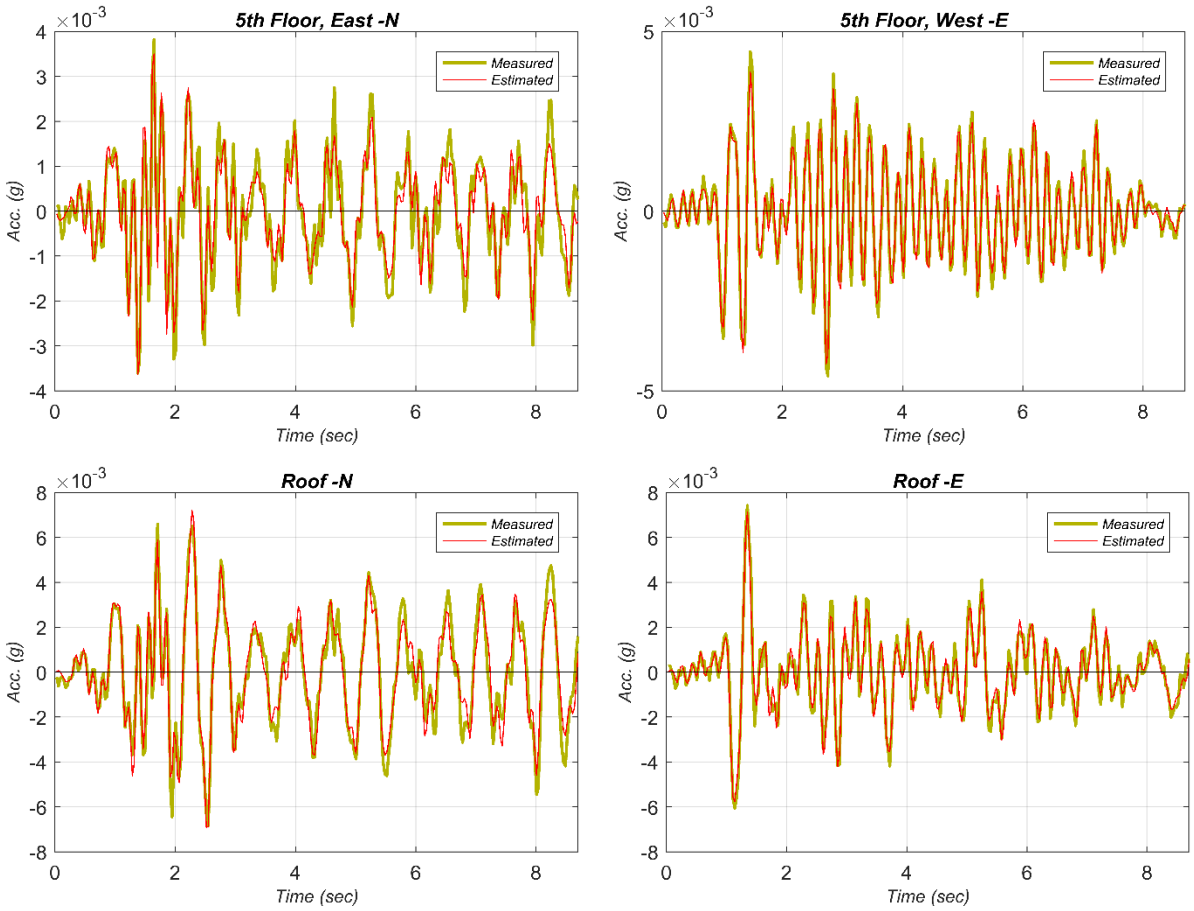

Figure 14: Comparison of the measured structural responses with the structural responses predicted using the final estimate of soil parameters and FIM.

We first developed a detailed FE model of the Millikan library structure. Through an identifiability analysis, we determined the sensitivity of the structural response to various model parameters, and selected a set of parameters that were likely to be identifiable. Since, we used the 2002 Yorba Linda earthquake data, which is a low-amplitude earthquake, we used a linear-elastic FE model of the building structure. At the first step, we performed an input-output model updating to estimate the model parameters related to the structural system. For this purpose, we utilized the foundation motion, measured on the foundation level, and the output response of the structure to estimate six structural model parameters. At the second step, we performed and output-only model updating to estimate the foundation input motions (FIM) and the parameters characterizing the stiffness and viscosity of the soil spring and dashpots. For this purpose, the structural model parameters were fixed at the parameter estimates obtained from the input-output model updating step. Eight soil-related parameters and three components of the FIM were estimated using the recorded response of the structure during the Yorba Linda earthquake.

The objective of this study was to develop, verify, and validate a FE model updating capability that can be used with real-world data. The FE model updating is a tool to integrate

mechanics-based models with measurement data obtained from real world, to reduce the uncertainties in the model and thus, provide more accurate information about the system properties, behavior, and its parameters. The long-term goal of this research initiative is to use this approach for investigating the soil model parameters that are used to model the inertial soil-structure interaction effects.

Acknowledgements

This study was supported partially by the California Geological Survey through Contract # 106-987. This support is gratefully acknowledged. Any opinions, findings, conclusions or recommendations expressed in this study are those of the authors and do not necessarily reflect the views of the sponsoring agency.

References

[1] ASCE, "Minimum Design Loads for Buildings and Other Structures, ASCE/SEI 7-10," American Society of Civil Engineers, Reston, VA, 2010.

[2] PEER, "Guidelines for Performance-Based Seismic Design of Tall Buildings," Pacific Earthquake Engineering Research Center as part of the Tall Buildings Initiative, University of California, Berkeley, CA, 2010.

[3] NEHRP Consultants Joint Venture, "NIST GCR 12-917-21," National Institute of Standards and Technology, Gaithersburg, MD, 2012.

[4] J. M. Roesset, "A review of soil-structure interaction," in *Soil-structure interaction: The status of current analysis methods and research, Rep. No. NUREG/CR-1780 and UCRL-*, Washington, D.C., U.S. Nuclear Regulatory Commission, 1980.

[5] H. Ebrahimian, R. Astroza and J. P. Conte, "Extended Kalman filter for material parameter estimation in nonlinear structural finite element models using direct differentiation method," *Earthquake Engineering and Structural Dynamics,* vol. 44, no. 10, pp. 1495-1522, 2015.

[6] R. Astroza, H. Ebrahimian and J. P. Conte, "Material Parameter Identification in Distributed Plasticity FE Models of Frame-Type Structures Using Nonlinear Stochastic Filtering," *ASCE Journal of Engineering Mechanics,* vol. 141, no. 5, pp. 04014149 1-17, 2015.

[7] H. Ebrahimian, R. Astroza, J. P. Conte and C. Papadimitriou, "Bayesian optimal estimation for output-only nonlinear system and damage identification of civil structures," *Structural Control and Health Monitoring,* vol. in press, 2017.

[8] A. K. Chopra, Dynamics of Structures: Theory and Applications to Earthquake Engineering, Englewood Cliffs, N.J.: Prentice-Hall, 4th Ed., 2012.

[9] J. L. Beck and L. S. Katafygiotis, "Updating Models and their Uncertainties. Part I: Bayesian Statistical Framework," *ASCE Journal of Engineering Mechanics,* vol. 124, no. 4, pp. 455-461, 1998.

[10] J. L. Beck, "Bayesian System Identification based on Probability Logic," *Structural Control and Health Monitoring,* vol. 17, no. 7, p. 825–847, 2010.

[11] D. Simon, Optimal State Estimation: Kalman, H-Infinity, and Nonlinear Approaches, Hoboken, NJ: John Wiley & Sons, 2006.

[12] S. J. Julier and J. K. Uhlmann, "A new extension of the Kalman filter to nonlinear systems," in *11th International Symposium on Aerospace/Defense Sensing, Simulation and Controls*, Orlando, FL, 1997.

[13] E. A. Wan and R. van der Merwe, "The unscented Kalman filter for nonlinear estimation," in *IEEE 2000 Adaptive Systems for Signal Processing, Communications, and Control Symposium*, Lake Louise, Canada, 2000.

[14] R. Astroza, H. Ebrahimian and J. P. Conte, "Batch and Recursive Bayesian Estimation Methods for Nonlinear Structural System Identification," in *Risk and Reliability Analysis: Theory and Application – In Honor of Prof. Armen Der Kiureghian*, Springer, 2016.

[15] R. Astroza, H. Ebrahimian, Y. Li and J. P. Conte, "Bayesian Nonlinear Structural FE Model and Seismic Input Identification for Damage Assessment of Civil Structures," *Mechanical Systems and Signal Processing,* vol. 93, no. 1, p. 661–687, 2017.

[16] S. F. Ghahari, F. Abazarsa, O. Avci, M. Çelebi and E. Taciroglu, "Blind Identification of the Millikan Library from Earthquake Data Considering Soil–Structure Interaction," *Structural Control and Health Monitoring,* vol. 23, pp. 684-706, 2016.

[17] Computers and Structures, Inc., "SAP2000," [Online]. Available: https://www.csiamerica.com/products/sap2000. [Accessed 09 2017].

[18] OpenSees, "Open System for Earthquake Engineering Simulation," [Online]. Available: http://opensees.berkeley.edu/. [Accessed 08 2017].

[19] X. Lu, L. Xie , H. Guan , Y. Huang and X. Lu, "A Shear Wall Element for Nonlinear Seismic Analysis of Super-tall Buildings using OpenSees," *Finite Elements in Analysis and Design,* vol. 98, pp. 14-25, 2015.

[20] CESMD - A Cooperative Effort, "Center for Engineering Strong Motion Data," [Online]. Available: https://www.strongmotioncenter.org/. [Accessed 09 2017].

[21] H. Ebrahimian, "Nonlinear Finite Element Model Updating for Nonlinear System and Damage Identification of Civil Structures," Ph.D. Dissertation, UC San Diego, La Jolla, CA, 2015.

[22] J. Kuroiwa, "Vibration Tests of a Multistory Building," Ph.D. Dissertation, California Institute of Technology, Pasadena, California, 1967.

[23] P. Jenning and J. Kuroiwa, "Vibration and Soil–Structure Interaction Tests of a Nine-Story Reinforced Concrete Building," *Bulletin of the Seismological Society of America,* vol. 3, no. 891-916, p. 58, 1968.

[24] J. Luco, M. Trifunac and H. Wong, "On the Apparent Change in Dynamic Behavior of a Nine-Story Reinforced Concrete Building," *Bulletin of the Seismological Society of America,* vol. 77, no. 6, p. 1961–1983, 1987.

[25] A. Belleri, M. Torquati, A. Marini and P. Riva, "Horizontal Cladding Panels: In-plane Seismic Performance in Precast Concrete Buildings," *Bulletin of Earthquake Engineering,* vol. 14, no. 4, pp. 1103-1129, 2016.